# Phase Separation for Open Circuit Fault-tolerance in a Multirotor Air Vehicle Propulsion Chain Using Switched Reluctance Machines

Marcin BICZYSKI[1,2], Rabia SEHAB[1], Guillaume KREBS[3], James WHIDBORNE[2]
[1]ESTACA - Campus Ouest, Rue Georges Charpak, 53061 Laval, France
[2]Cranfield University, College Road, MK43 0AL Cranfield, UK
[3]Université Paris-Saclay, CentraleSupélec, CNRS, Laboratoire de Génie Electrique et Electronique de Paris, 91192, Gif-sur-Yvette, France. Sorbonne Université, CNRS, Laboratoire de Génie Electrique et Electronique de Paris, 75252, Paris, France

**ABSTRACT – Electric aircraft nowadays use almost exclusively permanent magnet motors, which have good performance but open circuit faults render them inoperable. This is especially dangerous in multirotor drones, which are forced to utilize hardware redundancy by doubling the number of motors. A potential, more sustainable, alternative is to use independent phases within one motor, which enables the motor to operate in a reduced capacity after fault. This is verified through the design and testing of a switched reluctance motor for air vehicle applications. The actuating system is able to deliver more thrust than is required for hover even with 2 phases inoperable. This approach, coupled with fault-tolerant control, can be treated as an alternative to motor redundancy in safety critical systems.**

***Keywords – Fault-tolerance, open circuit fault, phase separation, reliability, switched reluctance.***

## 1. INTRODUCTION

In electric aircraft, e-VTOL, drones and other air vehicles, the propulsion chains are usually based on Permanent Magnet Synchronous Machines (PMSM) or Brushless DC (BLDC) motors. These machines are well suited to these applications because of their performance but they are not fault-tolerant by default. Common faults include inter-winding short circuit, transistor shoot-through and open circuit. Especially the latter are of high severity, as they can severely disable the motor. This is because of the reuse of coils (connected in a wye configuration) during different stages of the work-cycle [1]. Such faults may reduce the number of controllable degrees of freedom of the vehicle [2], potentially leading to crashes. To ensure reliability and safety of air vehicles during flight, multiple approaches such as over-sizing, fault-tolerant control or parachute systems [3] can be adopted.

One of the most common ones for air vehicles is the hardware redundancy. For example, in multirotor drones and e-VTOLs, two propulsion chains of 4 motors each can be used in such a way, that the single chain remaining after a failure has enough output for hove and safe landing of the vehicle. This way, the flight controller can isolate the faulty motor with its own control when a fault is detected. This has a downside of force fight [4] when using a single propeller or increased cost and propwash effects when using a dedicated propeller for each motor. A particular form of redundancy is also achieved when using two sets of coils on a single stator, with a common rotor [5]. This combines the fault-tolerance of the conventional approach with cost reduction, as only a single motor and propeller are used. However, this solution is not common in multirotor drones, as it increase the weight of the motor assembly and requires more complex heat dissipation solutions.

To improve the reliability of air vehicles, without using hardware redundancy, the approach of introducing phase separation within each motor is proposed, which should lead to increased fault-tolerance against open-circuit faults. This approach is characteristic of Switched Reluctance (SR) machines that exhibit significant mechanical, electrical, thermal and magnetic separation of the phases [6]. Thanks to the lack of rare-earth magnets SR motors are more sustainable, which is a sought-after quality nowadays, thus making SR motors a more interesting candidate. Therefore, a set of SR motors for a 10-kg multirotor drone application was designed and tested in healthy and faulty operation modes. It needs to be noted, however, that such separation can also occur within some multiphase PM motors [7].

## 2. PROPOSED VEHICLE AND PROPULSION CHAIN

A 10-kg consumer-grade multirotor drone was chosen as the demonstrator testbed. The model selected is Starfury X8 [1] by Pilgrim Technology - a multi-mission unit, with eight co-axial rotors arranged in the *x*-configuration, capable of carrying up to 5 kg of payload. In such vehicle the effects of a motor failure are the most dangerous and the effects of hardware redundancy and phase separation can be directly compared. A new design of a switched reluctance motor (Figure 1) is carried out considering mass constraint and performances related to air vehicles. As SR

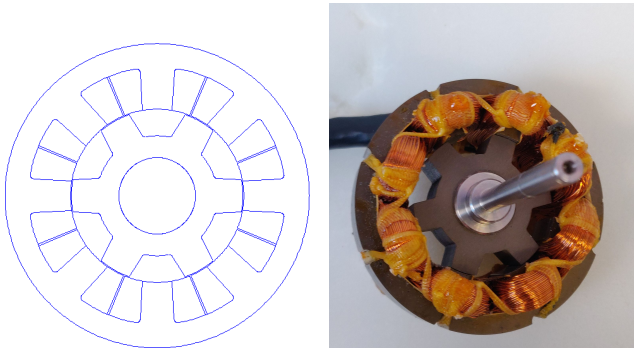

(a) Proposed motor geometry. (b) Manufactured assembly with shaft.

FIG. 1. Switched reluctance motor for multirotor air vehicles applications.

machines are robust and of fault-tolerant design, the new propulsion chain of air vehicles is composed of four SR motors where hardware redundancy is not considered. Therefore, it is designed

1. https://www.pilgrim-technology.com/starfury-x8/

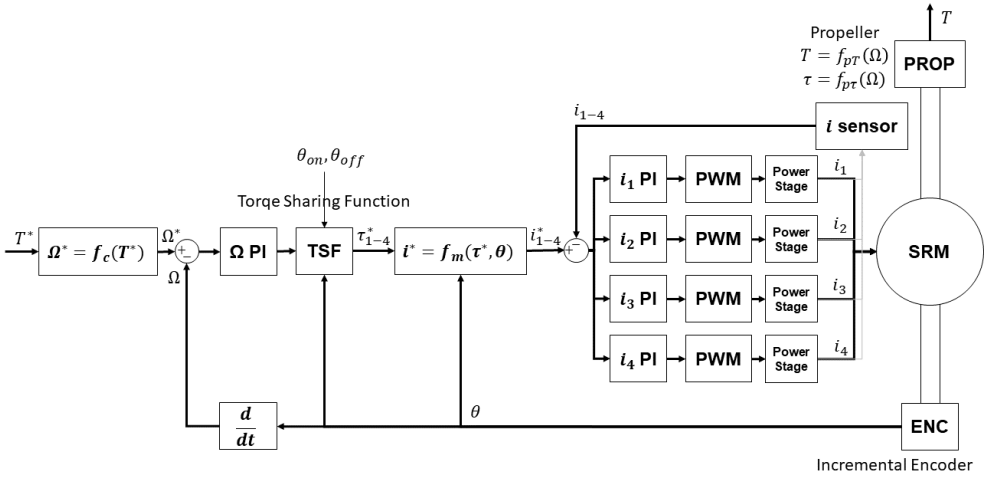


FIG. 2. Actuating system diagram.

such as it can replace an eight motor redundant propulsion system, while achieving similar power and weight. However, due to the simplicity of the design, the expected costs are lower and the manufacture is more sustainable. The proposed propulsion chain to improve reliability of air vehicles is based on a designed 8/6 SR motor where the number of phases ($m = 4$) is chosen so that the loss of two phases still allows provision of the minimum amount of thrust to enable hover. The design considers the mass constraint and performances related to air vehicles, such as the motor geometry had to be optimized specifically for the vehicle, as described in [8]. The main parameters of the motor are summarized in Table 1.

| | |
|---|---|
| Phases | 4 |
| Stator teeth | 8 |
| Rotor teeth | 6 |
| Outer Diameter | 71.0 mm |
| Stator bore | 40.4 mm |
| Airgap | 0.2 mm |
| Voltage | 22.2 - 25.2 V (6S LiPo) |
| Rated power | 640 W |
| Rated speed | 5500 RPM |
| Rated torque | 1.1 Nm |
| Rated current | 32 $A_{r.m.s.}$ |
| Rated efficiency | 73% |

TABLE 1. Summary of SR motor parameters.

The design process has resulted in a SR machine of 601 g (stator - 275 g, rotor and shaft - 161 g). Compared with 296 g of the reference off-the-shelf BLDC motor, the designed motor is considerably heavier. When factoring in the redundant setup and speed controller hardware (109 g in case of one BLDC motor ESC), the SR motor propulsion requires the electronics (asymmetric half-bridge DC converter) to be under 287 g for the actuating systems to be matched in both power and weight.

## 3. OPERATING MODES AND RESULTS

The control strategy selected for the velocity control is based on two cascade control loops : velocity and current. Figure 2 shows the block diagram of this control strategy. Controller parameters were chosen to minimize settling time and steady state error of output thrust, but due to high complexity of the model and time constraint, the values were found with low precision. It was also noticed that the fault-tolerance qualities were negligibly affected by the controller's tuning.

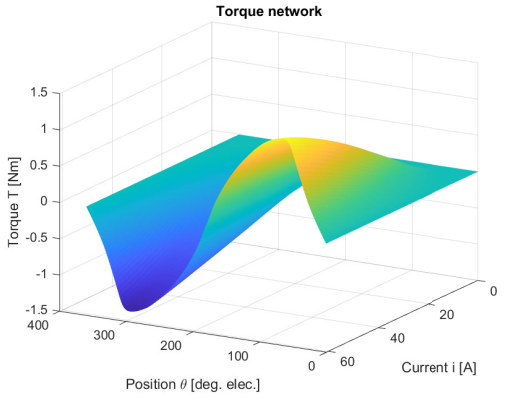


(a) Torque characteristic $T = f_t(\theta, i)$.

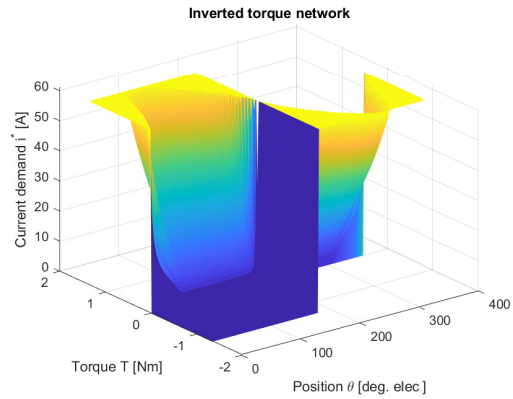


(b) Inverse torque characteristic $i^* = f_m(T, \theta)$.

FIG. 3. Nonlinear torque characteristic of the designed SR motor and its inverse.

The input torque demand is additionally conditioned using a simplified system model $\Omega^* = f_c(T^*)$ as a look-up table to obtain motor velocity demand. This approach is especially useful when comparing with reference motors.

The velocity control loop provides the total torque demand to a torque sharing function (TSF) in charge to generate torque demand for each phase. As torque feedback is not available (lack

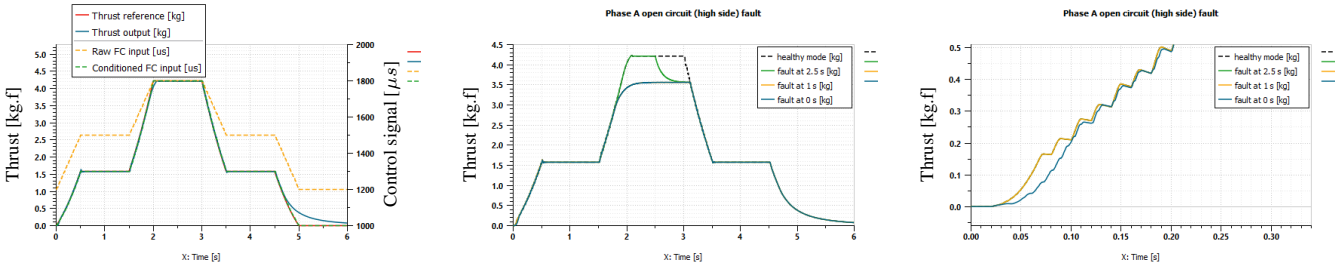


(a) Healthy mode.

(b) Open circuit fault in phase A.

(c) Open circuit fault in phase A at startup.

FIG. 4. Switched reluctance motor in a healthy mode and single phase fault operation mode.

of suitable sensor), the TSF uses a simple mathematical equation based on [9] to keep the average demand constant and minimize torque ripple :

$$TSF(\theta) = \begin{cases} 0, & (0 \leq \theta \leq \theta_{on}) \\ \frac{T_e}{2} - \frac{T_e}{2}\cos\frac{\pi}{\theta_{ov}}(\theta - \theta_{on}), & (\theta_{on} \leq \theta \leq \theta_{on} + \theta_{ov}) \\ T_e, & (\theta_{on} + \theta_{ov} \leq \theta \leq \theta_{off}) \\ \frac{T_e}{2} + \frac{T_e}{2}\cos\frac{\pi}{\theta_{ov}}(\theta - \theta_{off}), & (\theta_{off} \leq \theta \leq \theta_{off} + \theta_{ov}) \\ 0, & (0 \leq \theta_{off} + \theta_{ov} \leq \theta_p) \end{cases} \quad (1)$$

where $\theta_{on}, \theta_{off}, \theta_{ov}$ and $\theta_p$ are firing, commutation, overlap and rotor period angles respectively. From each phase's torque demand, a phase current demand is calculated using the inverse of the nonlinear torque characteristics given in Figure 3. It was obtained from repeated simulations, as a part of the motor design process.

The deduced current demand values are finally provided to the four current control loops to generate PWM signals of the converter (Power stage block in Figure 2). The topology used is the asymmetric bridge converter, shown in Figure 5, as it offers the compromise between the number of transistors (thus overall weight) and preserving the phase separation [10]. Although current direction does not matter in SR motors, the ability to conduct in both directions (with optional zero voltage allowing for diode freewheeling to lessen the burden on switches) is required to quickly build up and dissipate current in the coils to achieve higher motor speed.

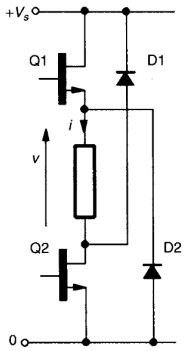


FIG. 5. One leg of the asymmetric bridge converter [11].

The phase separation is present in the motor (electrical, magnetic, and thermal), in the converter (electrical) and in the control system. This could further be enhanced by implementing the independent current control loops on separate microcontrollers, but was not planned for cost effectiveness. Based on the presented control strategy and converter setup, a simulation was carried out in healthy and faulty operation modes using the model and the data of the manufactured SR motor and the propeller load modeled using two look-up tables : $T = f_{pT}(\Omega)$ and $\tau = f_{p\tau}(\Omega)$. The numerical data is taken from the measurement of the demonstrator vehicle propeller (T-motor P18x6.1) on the ground test-bench and shown in Figure 6.

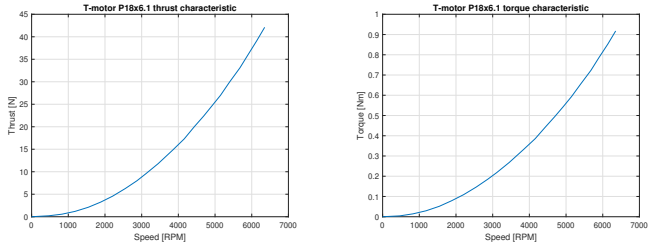


(a) Propeller thrust characteristic $T = f_{pT}(\Omega)$.

(b) Propeller torque characteristic $\tau = f_{p\tau}(\Omega)$.

FIG. 6. T-motor P18x6.1 propeller characteristics.

### 3.1. *Healthy mode*

The actuating system (including propeller and encoder) has been simulated in Simcenter Amesim 17 such as it accelerates to 50% throttle, through to 80% throttle, decelerates back to 50% and finishes at closed throttle, as shown in Figure 4a. The input (control) signal is designed to resemble the in-vehicle environment, thus it is defined as a typical servo motor signal of 1000-2000 $\mu s$ pulse in a 20 ms period (frequency of 50 Hz). Figure 4c shows that the achieved dynamics of the system are sufficient for such constraints if not overtuned and following the reference signal too closely to the point of introducing unwanted oscillations.

The performance of the reference motor in healthy mode was measured on a ground test-bench in a laboratory environment. The gathered data is compared to the simulated performance of the SR motor in Figure 8 (SR motor in blue, BLDC motor in red). The dynamics of the ESC for the BLDC setup was modeled as input signal conditioning to visually match output characteristics. This way, the result are matched with the only clear discrepancy is the saturation of SR motor thrust around 4.1 kg.f due to the limitation of the torque characteristic lookup table.

There is no breaking operation, so the main source of deceleration is aerodynamic drag, which at low speeds is less pronounced, thus the deviation in speed (and thrust) in the last stage of the test. That behavior, however, is fully expected and also present in conventional solutions, as seen in Figure 8.

### 3.2. *Faulty mode*

Faulty mode was tested in configurations with one, two and three phases disabled as a inter-winding open circuit. Figure 4b shows the decrease in maximum thrust with one phase disabled is less than 25%. In addition, the impact on acceleration capability and start-up time is minimal (Figure 4c). However, although this figure shows a satisfactory tracking performance, the discretized setpoint signal translates to an irregular output curve.

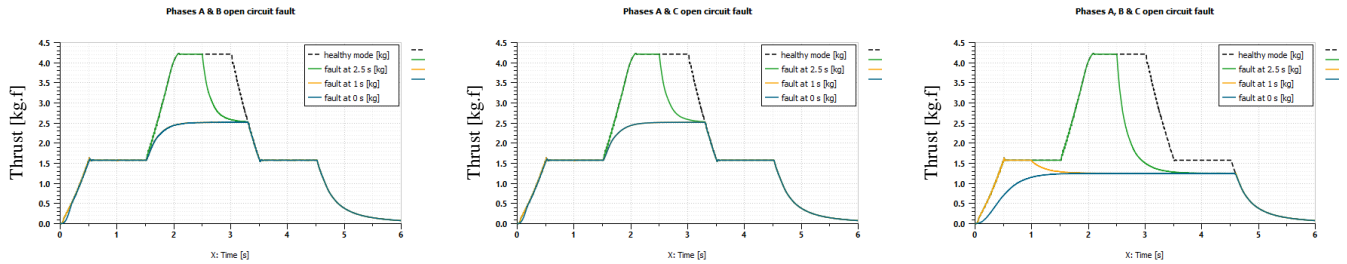


(a) Open circuit fault in adjacent phases A and B. (b) Open circuit fault in opposite phases A and C. (c) Open circuit fault in phases A, B and C.

FIG. 7. Switched reluctance motor in a multiple phase fault operation mode.

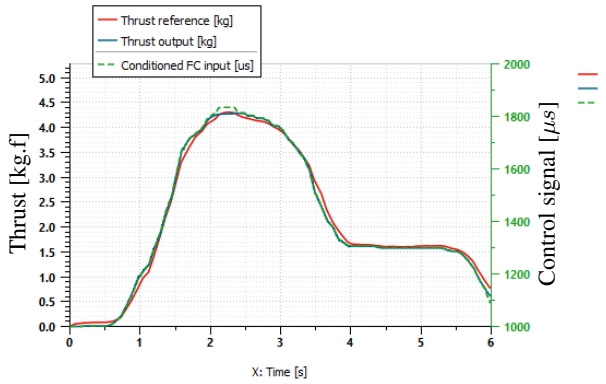


FIG. 8. Comparison of a SR motor and BLDC motor in healthy mode.

In a physical system this may not pose a problem due to additional sources of damping present, such as propeller aerodynamics (which is modeled in a very basic capacity in the simulation).

Figure 7 confirms that despite two open-phase faults present, a 4-phase SR motor can still operate with over 50% thrust capacity, which is sufficient for hover and safe landing of the aircraft. This is true for faults in adjacent, as well as opposite phases. As expected, this capability is not maintained when losing three phases. In this case, the acceleration capability is severely degraded, which may affect the dynamics of the whole vehicle leading to the loss of control.

The simulation setup allows for precise control of the initial conditions, such as the motor is always able to start from zero speed. It needs to be noted that in the real case, the loss of each phase reduces the self-starting capability and advanced control strategies must be used to compensate.

Open circuit faults are analyzed in [1, 12] in regards to typical BLDC motors, where due to the wye winding configuration, a fault in a transistor reduces available torque (thus available thrust) by a one third. A fault in the motor winding or the connecting wire reduces the motor to a 1-phase, resulting in even greater decrease in thrust. It was shown that in phase-separated SR motors the loss of each phase results mainly in reduction of maximum thrust (and torque) capacity of less than 25%, which is an improvement over BLDC motors in both disabled transistor and disabled winding scenarios, even when adjusted for the difference in phase count.

## 4. CONCLUSIONS

In healthy and faulty operation modes, the designed SR motors are able continue operation despite open-circuit faults during a flight. This is a direct consequence of the motor's stator phases being independent. Each phase is supplied and controlled separately using its own current sensor and current control loop. This arrangement allows to replace redundant motors with fault-tolerant motors for a potential decrease in weight and cost, and with the increase in sustainability. Although currently the motor obtained in this work is considerably heavier than conventional counterparts (because of the immaturity of the technology), phase separation principle can contribute to fault-tolerance regardless of motor type. This way, enhanced safety can be achieved alongside good performance and low weight.

## 5. REFERENCES


[1] R. Spée and A. K. Wallace, "Remedial Strategies for Brushless DC Drive Failures," *IEEE Transactions on Industry Applications*, vol. 26, no. 2, pp. 259–266, 1990.

[2] Q. L. Zhou, Y. Zhang, C. A. Rabbath, and D. Theilliol, "Design of feedback linearization control and reconfigurable control allocation with application to a quadrotor UAV," *Conference on Control and Fault-Tolerant Systems, SysTol'10 - Final Program and Book of Abstracts*, no. 514, pp. 371–376, 2010.

[3] J. D. Littell, "Challenges in vehicle safety and occupant protection for autonomous electric vertical take-off and landing (Evtol) vehicles," in *AIAA Propulsion and Energy Forum and Exposition*, no. August, pp. 1–16, AIAA, 2019.

[4] P. Estival, R. Sehab, G. Krebs, and B. Barbedette, "Force fight and its elimination in a prototype of a redundant direct-drive avionic actuator," *Applied Sciences (Switzerland)*, vol. 10, no. 23, pp. 1–20, 2020.

[5] Z. Fu, X. Liu, and J. Liu, "Research on the fault diagnosis of dual-redundancy BLDC motor," *Energy Reports*, vol. 7, pp. 17–22, 2021.

[6] G. J. Atkinson, J. W. Bennett, B. C. Mecrow, D. J. Atkinson, A. G. Jack, and V. Pickert, "Fault tolerant drives for aerospace applications," in *2010 6th International Conference on Integrated Power Electronics Systems*, 9 2010.

[7] M. Villani, M. Tursini, G. Fabri, and L. Castellini, "Multi-phase permanent magnet motor drives for fault-tolerant applications," in *2011 IEEE International Electric Machines & Drives Conference (IEMDC)*, pp. 1351–1356, IEEE, 5 2011.

[8] M. Biczyski, R. Sehab, G. Krebs, J. F. Whidborne, and P. Luk, "Designing Low-weight Switched Reluctance Motors for Electric Multirotor Propulsion System," in *International Conference on More Electric Aircraft (MEA2021)*, no. P2-20, (Bordeaux, France), pp. 1–5, 2021.

[9] E. Gouda, M. Hamouda, and A. R. Amin, "Artificial intelligence based torque ripple minimization of Switched Reluctance Motor drives," *2016 18th International Middle-East Power Systems Conference, MEPCON 2016 - Proceedings*, pp. 943–948, 2017.

[10] R. Sehab, A. Akrad, and Y. Saadi, "Super-Twisting Sliding Mode Control to Improve Performances and Robustness of a Switched Reluctance Machine for an Electric Vehicle Drivetrain Application †," *Energies*, vol. 16, 4 2023.

[11] T. J. E. Miller, *Electronic Control of Switched Reluctance Machines*. Elsevier, 2001.

[12] H. He and J. Yang, "Diagnosis strategy of switch open circuit fault in brushless dc motor drives," in *2017 3rd IEEE International Conference on Control Science and Systems Engineering (ICCSSE)*, pp. 355–358, IEEE, 8 2017.